Solid State Communications 229 (2016) 49–52

Contents lists available at ScienceDirect

Solid State Communications

journal homepage: www.elsevier.com/locate/ssc

Fast-track Communication

Defects, a challenge for graphene in flexible electronics

A.J.M. Giesbers [a,*], P.C.P. Bouten [a], J.F.M. Cillessen [a], L. van der Tempel [a], J.H. Klootwijk [a], A. Pesquera [b], A. Centeno [b], A. Zurutuza [b], A.R. Balkenende [a]

[a] Photonic Materials and Devices, Philips Research, High Tech Campus 4, 5656 AE Eindhoven, the Netherlands
[b] Graphenea, S.A. A75022608 Tolosa Hiribidea 76, 20018 Donostia-San Sebastian, Spain

ARTICLE INFO

Article history:
Received 14 August 2015
Received in revised form
2 January 2016
Accepted 4 January 2016
Available online 8 January 2016

Keywords:
Graphene
Flexible
Gas barrier
Defects
Water vapor transmission rate
Stress
Bending

ABSTRACT

In this work we present the effect of defects in graphene on its potential for application in flexible electronics. We visualize defects at the grain boundaries, transfer defects and local atomic defects. We show that these defects are currently determining the gas barrier properties of graphene. Under strain up to only 2% we show that these defects lead to cracks in the graphene thereby deteriorating its conductivity.

1. Introduction

Graphene is a material of many superlatives such as high mobility [1], superior thermal conductivity [2], large maximum allowable strain [3] and extremely low permeability [4]. These properties lead to visions of many potential applications. However, some major challenges must be tackled to enable industrial application. One of the most significant issues in large area graphene are defects. We will quantify the effect of these defects for flexible graphene electrodes and graphene based gas barriers. Further, a method to visualize the defects is presented. We will show that the structural defect density can locally (um^2-scale) be as high as 10^{10} cm^{-2} in good quality transferred CVD graphene. The defects strongly reduce the applicable strain in flexible applications from the theoretical 20% strain to about 1.2% strain. Also the barrier properties of graphene are severely reduced: the water vapor transmission rate is $3 \cdot 10^{-2}$ g/m^2/day at 50% humidity and 20 °C, more than 4 orders below the intrinsic potential.

2. Defects in graphene

To visualize the structural defects in graphene a CVD grown graphene layer [5] is covered by a thin layer of gold (Au) (25 nm) and transferred (top down) to a Si/SiO_2 wafer. This leads to a sample consisting of a Si/SiO_2 substrate followed by a thin Au layer covered by a single graphene top layer. Exposing this sample to a potassium iodide (KI) solution etches pinholes in the Au layer through those defects in the graphene layer that are large enough for the KI-etchant to pass, whereas the rest of the Au is protected by the graphene crystal lattice. The etch time was typically 2 min at a temperature of 20 °C with an etch speed of $v_{etch} = 10$ nm/min. The pin holes in the thin Au layer result in a large contrast in scanning electron micrographs making this a powerful tool to visualize very small structural defects. Fig. 1 presents typical results after etching showing three distinct types of etch pits. In total 3 different samples were analyzed with this technique with a total area of 3 cm^2.

Agglomerates of etch pits like indicated in area I in Fig. 1 are observed over the entire sample. Typically in dimensions of an area of a few tens of um^2 in an area of a few thousand um^2 (Fig. 1 is a typical example). The density of etch pits in these areas can be as high as 10^{10} cm^{-2} with etch pit sizes ranging from 40 nm to a few 100 nm. The sample is further covered by a network of etch pits (area II in Fig. 1) with pit sizes similar to the ones in the agglomerates. Typically the etch pit lines enclose unaffected areas of 5–10 μm in diameter. Finally, we observe large etch pits, up to

* Corresponding author.
E-mail addresses: jos.giesbers@philips.com (A.J.M. Giesbers), ruud.balkenende@philips.com (A.R. Balkenende).

http://dx.doi.org/10.1016/j.ssc.2016.01.002
0038-1098/

several micrometers in size, scattered over the sample like the one indicated in area III in Fig. 1. These last ones are so large that they must be ascribed to areas where graphene is missing e.g. due to incomplete graphene growth or transfer defects. The smaller etch pits, of about 40 nm in size, likely originate from point defects and are ascribed to atomic defects, considering etch rate (10 nm/min.) and time (2 min). The atomic pinhole size [6] of about 3 Å in case of one missing atom is in theory large enough for water (~2 Å) and the etchant molecules (~2 Å) to pass, whereas the carbon-hexagon in graphene with a diameter of 2.1 Å is impermeable. At this point however we cannot rule out that the expected atomic defect grew larger during e.g. etching of the Cu-substrate in $FeCl_3$ [7] or due to the transfer itself where additional bonds could be broken at the weaker defect sites [8] resulting in nanopores at these sites. The irregular shape of the slightly larger etch pits suggest groups of atomic defects where the crystal lattice is no longer a perfect honeycomb [6] or larger defects where locally multiple atoms are missing.

Accordingly, the lines forming a network of etch pits are ascribed to defects at the grain boundary lines. A high concentration of atomic defects is expected here due to a mismatch in the crystallographic orientation or alignment of the graphene lattice in the various grains [9]. This attribution is also in agreement with the typical grain size of 5–10 μm [9,10].

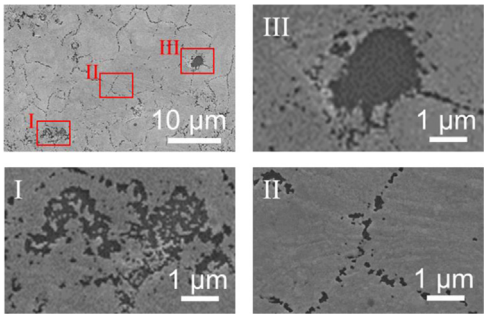

Fig. 1. Scanning electron micrographs of a graphene covered gold layer after etching in a KI solution (t=2 min, T=20 °C, v_{etch}=10 nm/min). Clearly visible are etch pits at the graphene grain boundaries, atomic defects and holes.

3. Defects and stress

In the next section we will discuss the effect of these defects on the strength of graphene. Graphene is considered an ideal transparent conductor in flexible applications due to its large elasticity. Its mechanical stiffness is 1 TPa, and the intrinsic breaking strength is 130 GPa, at 20% strain [3]. However, our measurements on large area graphene show that the electrical resistance already increases irreversibly at a strain of 1.2%. To measure this, CVD grown graphene was transferred to polyethylene naphthalate (PEN)-foil. The foil is 200 μm thick and has a RMS roughness of 5 nm. We use two types of samples, one with a 25 nm Au interlayer between the Au and the graphene to visualize the defects in a similar way as shown above, and one with the graphene directly on top of the PEN foil. The presence of the gold interlayer has no notable effect on the applied strain. The samples are controllably bent from flat down to 5 mm bending radius, while graphene's electrical resistance is monitored (inset Fig. 2a). In this way we can apply up to 2% strain, either tensile or compressive by bending upwards or downwards. For comparison we use the same PEN foil with a 50 nm ITO layer. At roughly 1% strain the ITO is known to form cracks perpendicular to the bending direction [11]. This leads to an abrupt and strong increase in the resistance of the layer as is evident from Fig. 2a. Reversing the strain will push the ITO at the cracks back into contact, almost restoring the resistance. In the case of graphene the resistance strongly increases for strains over 1.2% and does not return to its initial resistance value after relaxation, implying that the change is irreversible. Interestingly, the resistance perpendicular to the bending direction only increased by roughly half of that in the parallel direction, whereas at the start the material was isotropic.

The maximum strain observed for large area CVD graphene is much lower than reported previously for a single graphene flake (>20%) [3]. The probable cause for this is elucidated by the experiments with the gold interlayer and subsequent etching, showing the critical role of defects. Fig. 2a–b shows optical transmission micrographs visualizing the defect structure for three different strain levels. At 0% strain we observe the grain boundary structure as discussed above. When increasing the strain (Fig. 2c and d) the etching pattern changes from random grain boundaries to parallel etch lines. This is also clearly visualized in the SEM picture in Fig. 2e. Evidently, during bending crack lines are initiated

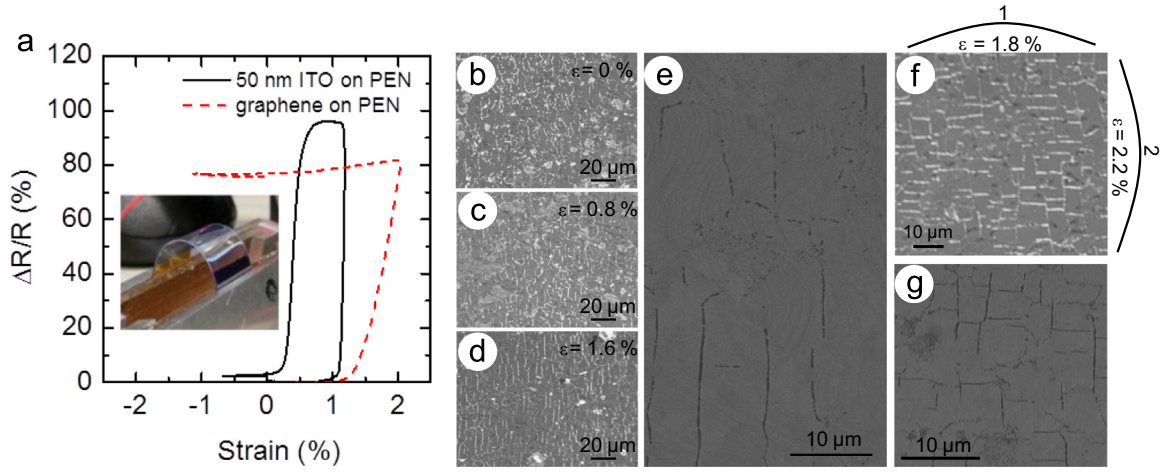

Fig. 2. (Color Online) (a) Resistance change as a function of the applied strain for ITO (solid black) and graphene (dashed red). The initial resistance of ITO=57 Ω and Graphene=1.43 kΩ. Inset: Photo of the automated bending setup, in which the resistance is measured while bending the graphene-on-PEN samples to a 5 mm radius. (b)–(d) Optical transmission images of graphene+Au etched in a KI solution after various applied strains. (e) Scanning electron micrograph of the etch pits in the gold after etching through bend graphene (1.6% strain). (f) Optical transmission image of a Au+graphene samples etched in KI-solution after two way bending. The markers on the side show the sequence of bending and the applied strain. (g) Scanning electron micrograph of the same sample.